IET Electric Power Applications

Research Article

Methods for overcoming misalignment effects and charging control of a dynamic wireless electric vehicle charging system

ISSN 1751-8660
Received on 7th August 2018
Revised 25th February 2019
Accepted on 10th April 2019
E-First on 30th April 2019
doi: 10.1049/iet-epa.2018.5509
www.ietdl.org

Merugu Kavitha[1] ✉, Dinkar Prasad[1], Phaneendra Babu Bobba[2]
[1]*Department of Electrical Engineering, Shiv Nadar University, Greater Noida, UP, India*
[2]*Department of Electrical and Electronics Engineering, GRIET, Hyderabad, Telangana, India*
✉ *E-mail: mk508@snu.edu.in*

Abstract: A new method of power control for wireless power transmission (WPT) system has been proposed and analysed. The circuit and method suggested in this study holds good promise of reducing switching loss in the high-frequency converter of WPT. The effect of misalignment between transmitter and receiver coils has been analysed and a simple remedial method has been proposed. The desirability of frequency tuning of converter's output voltage under varying degrees of misalignment has been highlighted. The conventional perturb and observe method for maximum power point tracking has been gainfully employed here to achieve the required frequency tuning of the proposed converter. The proposed methods are implemented and tested on laboratory scale. Some suggestions have been given for augmenting driver assistance system aimed at limiting lateral misalignment in dynamic WPT system. The suggested algorithm is tested in a laboratory environment using a simple communication system.

1 Introduction

Wireless power transmission (WPT) system is becoming popular for charging electric vehicles (EVs) [1–4]. The concept of dynamic wireless charging (DWC) system is also gaining importance [5, 6]. With advancement in image processing techniques, cloud computing and artificial intelligence the DWC systems may become a popular method for charging of EVs. The schematic arrangement of a typical DWC system for EV is shown in Fig. 1.

The DWC system consists of a string of transmitters deployed just below the road's surface and a receiver placed at the base of the vehicle chassis [7, 8]. The vehicle is supposed to be moving slowly and a driver assistance system is to guide the vehicle's path [9, 10]. Since the EV needs to be powered up during a short span of time, the power rating of charger circuit needs to be very high [11] and the charging system needs to be tolerant against minor misalignments between the transmitter and the receiver coils. To achieve high power charging, the losses in the power electronic converter needs to be minimised and a dynamic correction in charging current's frequency is required to offset the effect of coil's parameter changes under varying misalignment conditions. This paper dwells on the above two important issues of the DWC system and suggests some solutions which have been verified on a laboratory scale. Some preliminary ideas on driver assistance system for DWC have been given in the Appendix.

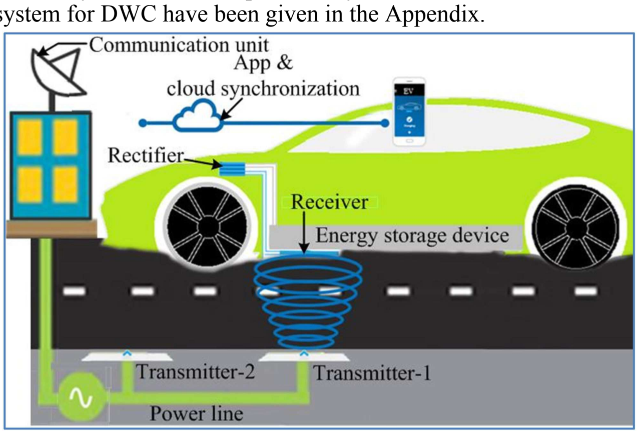

Fig. 1 *Schematic representation of DWC system for EV*

The paper is organised as follows: Section 2 presents the proposed WPT system and its theoretical analysis. Section 3 describes the effect of misalignments and frequency tuning methods. The frequency tuning logic is based on the popular perturb and observe (P & O) method used in connection with maximum power point tracking (MPPT) algorithm. Section 4 presents some experimental results. Section 5 concludes the paper.

2 Proposed WPT scheme

Fig. 2 shows the proposed WPT converter which feeds to the transmitter coil and associated compensation circuit. This converter topology, though described in the literature for various applications [12–15], has not been proposed much for wireless power charging, except by few researchers [16, 17]. The basic circuit topology resembles closely to the actively clamped resonant dc link converter proposed by Divan *et al.* [18, 19] for feeding the dc bus of an inverter. In the present paper, the authors have proposed an entirely different approach for making use of the clamped resonant dc link converter for powering WPT coil.

2.1 Power electronic converter for feeding the T_X coil

The circuit as shown in Fig. 2 produces a resonating voltage (V_{Cr}) across capacitor C_r. The operation of the resonant circuit is briefly reviewed here. For simplicity, first, the analysis is done under no-load condition (i.e. $I_1 = 0$) and later in (Section 2.4) the effect of the load current is considered. Figs. 2*a–c* show the operational part of the circuit during different modes of operation. The resulting waveforms of V_{Cr} and I_{Lr} are shown in Fig. 3. The time instants marked in Fig. 3 relate to different modes of circuit operation.

Mode-1 ($0 < t < t_2$) of the circuit operation starts when switch S_r turns off while carrying a current I_0. The operational part of the circuit during mode-1 is shown in Fig. 2*a*. At $t = 0$ (Fig. 3) capacitor voltage (V_{Cr}) = 0 and inductor current $I_{Lr} = I_0$. The current I_0 is adjustable. The expressions for V_{Cr} and I_{Lr} are given in

$$\begin{cases} V_{Cr}(t) = E(1 - \cos\omega t) + I_0\sqrt{L_r/C_r}\sin\omega t \\ I_{Lr}(t) = E\sqrt{C_r/L_r}\sin\omega t + I_0\cos\omega t \end{cases} \quad (1)$$

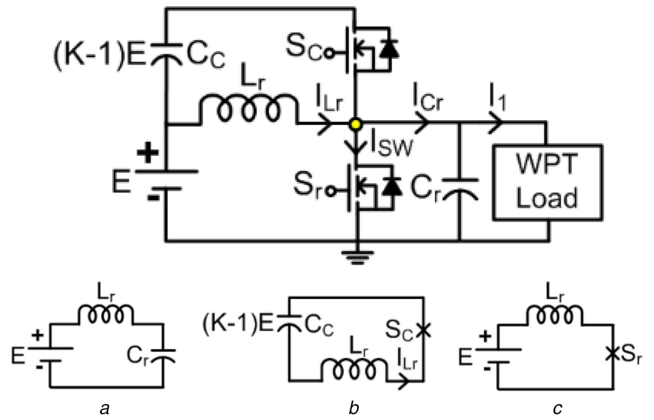

Fig. 2 *Power converter for WPT system*
(a)–(c) Different modes of circuit operation

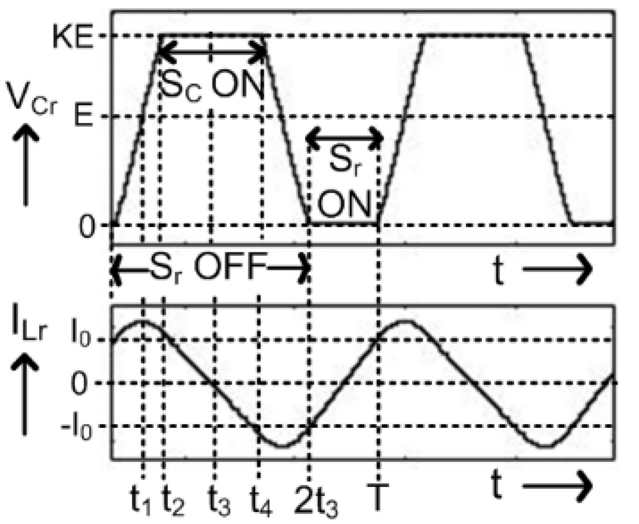

Fig. 3 *Typical waveforms of resonant circuit's voltage (V_{Cr}) and current (I_{Lr}) under no-load*

where V_{Cr} builds up to input voltage E at t_1 and clamping voltage KE at t_2. After reaching the clamping voltage, a further rise of V_{Cr} is prevented and the inductor current I_{Lr} is diverted to the large clamping capacitor C_C whose voltage is maintained at $(K-1)E$. Now the circuit operation changes to mode-2 with equivalent operational circuit given in Fig. 2*b*. During mode-2 ($t_2 < t < t_4$), initially, diode of switch S_C starts conducting and subsequently switch S_C is turned on. The inductor current (I_{Lr}) first discharges into the clamping capacitor C_C during ($t_2 < t < t_3$) and then starts charging in reverse direction during ($t_3 < t < t_4$). Charge transfer to C_C is monitored and S_C is turned off when net charge transfer equals zero. For the present analysis, C_C has been assumed to be very large such that the change in its voltage level is insignificant. However, in the practical implementation, the magnitude of C_C is taken only moderately large and net charge transfer is determined by the change in clamping voltage level. Mode-2 ends with turning off of S_C. During mode-2 the inductor current changes linearly as clamping voltage level is assumed constant. The circuit equation for mode-2 is given by

$$L_r \frac{dI_{Lr}}{dt} = (K-1)E \tag{2}$$

In mode-3 ($t_4 < t < 2t_3$), the equivalent operational circuit is same as in mode-1 (Fig. 2*a*) but with initial magnitude of $V_{Cr} = \text{KE}$ and I_{Lr} is in reverse direction. At the end of mode-3 ($t = 2t_3$) the capacitor voltage (V_{Cr}) resonates back to zero while I_{Lr} becomes $-I_0$. For zero magnitude of the load current the circuit is lossless and conditions at $t = 0$ and $2t_3$ are symmetrical. As V_{Cr} falls to zero switch S_r is turned on again and circuit enters into mode-4 of operation.

During mode-4 ($2t_3 < t < T$) the equivalent circuit is as shown in Fig. 2*c* and the inductor current rises linearly. The circuit equation is given by

$$L_r \frac{dI_{Lr}}{dt} = E \tag{3}$$

Mode-4 ends when magnitude of switch current reaches I_0 after which the next cycle is repeated.

It may be noted that V_{Cr} has a dc component too whose magnitude is the same as the input voltage E. Clamping voltage of V_{Cr} is chosen to maintain safe voltage stress across switch S_r. Both switches S_r and S_C operate under zero voltage switching condition.

The WPT system is fed with V_{Cr} voltage through a series compensation capacitors. The series capacitor blocks dc component of V_{Cr} and it simultaneously compensates for lagging power factor of WPT coil.

2.2 Inductively coupled WPT system

The inductively coupled WPT system is shown in Fig. 4*a* and its T-equivalent circuit is shown in Fig. 4*b*. The transmitter (T_X) and receiver (R_X) coils are assumed to be planer and are vertically apart by around 15 cm. T_X side is fed from output voltage (V_{Cr}) of the resonant converter and R_X side's voltage is rectified for charging the vehicle's battery/supercapacitor. In Fig. 4*a*, V_P denotes the fundamental frequency component of V_{Cr}. L_1 and L_2 are the self-inductances of transmitter and receiver coils. M is the mutual inductance and 'k' is the coupling factor. I_{L1} and I_{L2} are the instantaneous currents in transmitter and receiver coils, respectively. R_0 is the equivalent load on the receiver side.

Fig. 4*b* represents the equivalent circuit of coupled coils as seen from the transmitter side. L_{1L} and L_{2L} are the leakage inductances of T_X and R_X coils. L_M is the magnetising inductance (referred to transmitter side) and 'a' is the effective turns ratio. $\widetilde{R_0}$ denotes the equivalent reflected load as seen from the transmitter side. $Z_{1,\text{eqv}}$ is the equivalent impedance of the loaded coupled coils. The relation between these parameters is given by $L_1 = L_{1L} + L_M$, $L_2 = L_{2L} + (L_M/a^2)$, $L_M = \text{aM}$ and $k = M/\sqrt{L_1 L_2}$.

2.3 Method used for measuring coil parameters of WPT system

Experimental determination of the coil's parameters and equivalent load has been discussed in this subsection. The self-inductances of the transmitter (T_X) and receiver (R_X) side coils are measured by a precision *L–C–R* meter set at 100 kHz frequency. While measuring self-inductance of the T_X side, the R_X side coil is kept open and vice-versa. The self-inductance values are independent of alignment or position of coils. The values obtained from the meter are also verified in the actual setup of Fig. 5 by the voltage and current readings obtained. Here the coil's resistance and parasitic capacitances were neglected.

Mutual inductance (M) varies with the relative position between transmitter and receiver coils. However, M could not be measured directly with the available *L–C–R* meter and here the circuit of Fig. 5 was operated to get near sinusoidal voltage across the T_X coil while keeping R_X coil terminals open. The ratio of open circuit R_X coil voltage ($V_{2,\text{rms}}$) and T_X coil's current ($I_{1,\text{rms}}$) gives the product of M and angular frequency [i.e. $M = V_{2,\text{rms}}/(\omega_P I_{1,\text{rms}})$]. The magnitude of angular frequency (ω_P) is obtained with the help of oscilloscope.

The above procedure is repeated by replacing R_X side and T_X side coils. M observed from both sides is identical. After determining the self-inductances of T_X and R_X sides (L_1 and L_2,

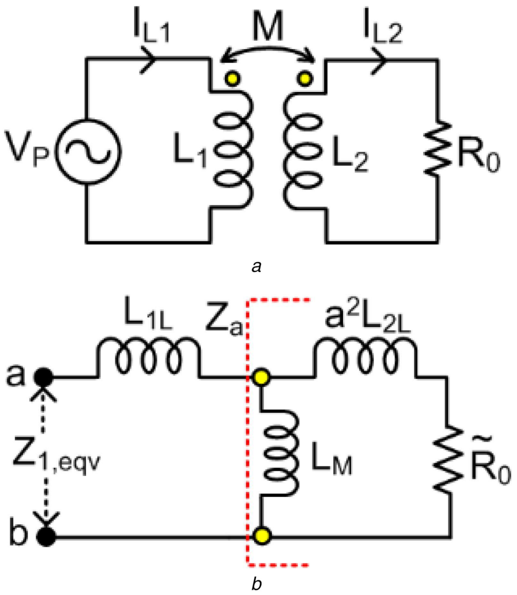

Fig. 4 *A typical wireless power transfer (WPT) system*
(a) Basic circuit of WPT System, ***(b)*** T-equivalent of WPT System

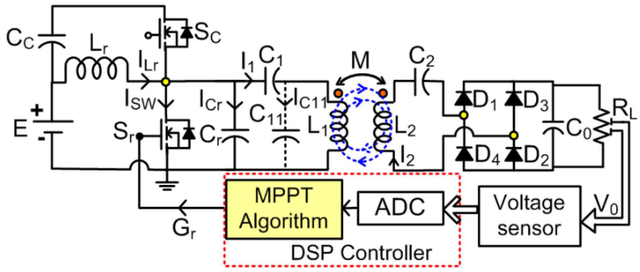

Fig. 5 *Frequency tuning arrangement of WPT system*

Table 1 Circuit parameters for experimental results

Parameter	Value	Unit
C_1 (T_X side capacitor)	8.050	nF
C_{11} (T_X side capacitor)	12.066	nF
C_2 (R_X side capacitor)	16.92	nF
C_C (clamping capacitor)	453	nF
L_r (resonant inductor)	28	μH
C_r (resonant capacitor)	60	nF
L_{1L} (T_X coil leakage ind.)	178.61	μH
L_{2L} (R_X coil leakage ind.)	246.37	μH
M (mutual ind.)	36.04	μH
a (turns ratio)	0.85	
R_L (load on R_X side)	100	Ω
E (input dc voltage)	200	V
I_0 (S_r current)	12	A
K (clamping volt. constant)		≈1.5

respectively), effective turns ratio 'a' was determined as $(a = \sqrt{L_1/L_2})$.

The load 'R_L' connected after rectifier in Fig. 5 appears as $(8/\pi^2)*R_L$ at the input of rectifier [20]. When seen from T_X side the effect of turns ratio needs to be considered too. Thus a load of 100 Ω ($=R_L$) appears to have a magnitude of 58.6 Ω ($=\widetilde{R_0}$) when referred to T_X side. Here the effective turns ratio is 0.85, as given in Table 1.

2.4 Compensation topology for WPT system

Owing to loose coupling between T_X and R_X coils, majority of magnetic flux produced by T_X coil will not link R_X coil. Mutual flux between them is only a small fraction of total flux. The leakage flux dominates. Due to the low coupling coefficient (k) between coils, the power factor of the uncompensated WPT system is poor. For enhanced efficiency of the system, compensation networks are put both on T_X and R_X sides. Various topologies of compensation networks have been proposed in the literature [21, 22] out of which series compensation topology has found more attention due to its simplicity and due to voltage-source nature of output from typical power electronic converters. In series–series

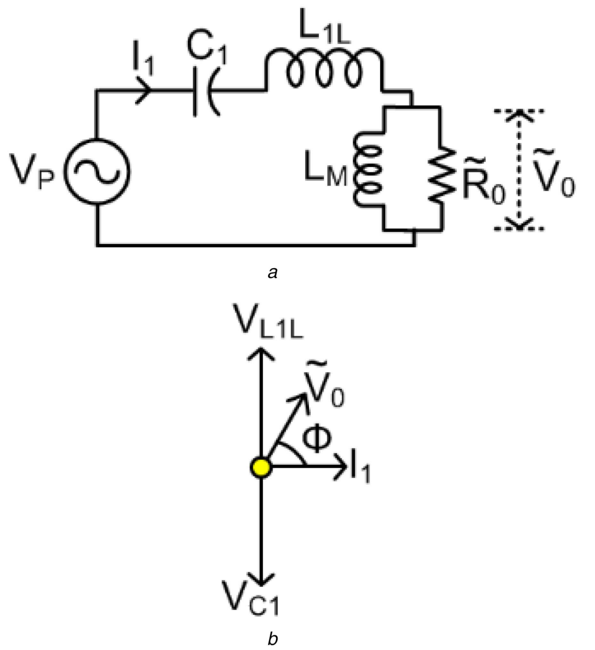

Fig. 6 *Equivalent circuit for loaded series-compensation topology*
(a) Equivalent circuit of series compensated WPT system, ***(b)*** Phasor diagram of circuit in Fig. 6*a*

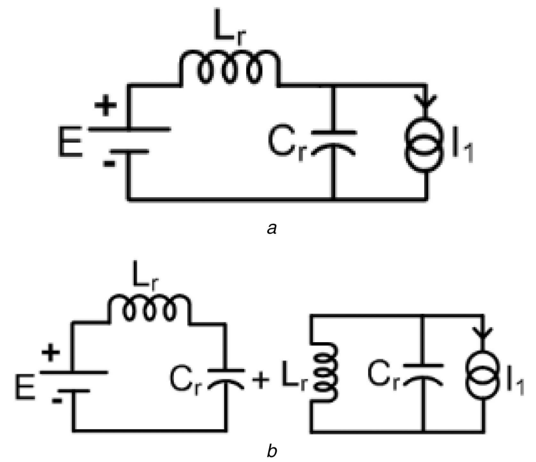

Fig. 7 *Equivalent converter configuration when S_r is off*
(a) Simplified representation of converter and WPT load, ***(b)*** Equivalent circuit decomposition for circuit of Fig. 7*a*

compensation topology, suitable compensating capacitors are put in series with the transmitter as well as receiver coils. Under ideal compensation, the resulting WPT system would appear as a unity power factor load to the ac voltage source. Assuming receiver side leakage inductance to be exactly compensated by its compensating capacitor the simplified equivalent circuit and corresponding phasor diagram have been presented in Figs. 6*a* and *b*. In Fig. 6*a* a sinusoidal input voltage is considered for the WPT system.

Under perfect receiver side compensation, voltage ($\widetilde{V_0}$) across mutual inductance (L_M) appears across equivalent load too. As seen from the transmitter side, $\widetilde{V_0}$ comes in series with voltages across L_{1L} and C_1. The reactive voltage components across both L_{1L} and L_M are cancelled by the voltage across C_1. The resulting phasor relations are given in

$$\begin{cases} V_{C1} = V_{L1L} + \widetilde{V_0}\sin(\phi) \\ \widetilde{V_0} = V_P/\cos(\phi) \end{cases} \quad (4)$$

where 'ϕ' $\left[= \tan^{-1}\left(\widetilde{R_0}/\omega_P L_M\right)\right]$ is the impedance angle of L_M and $\widetilde{R_0}$, 'ω_P' denotes angular frequency of V_P. The reflected load voltage ($\widetilde{V_0}$) is in phase with V_P but amplified by a factor ($1/\cos(\phi)$). After compensation, the WPT system is equivalent to a resistive load of magnitude $\cos(\phi)^2 * \widetilde{R_0}$ and the current (I_1) to transmitter coil equals $\left(V_P/\cos(\phi)^2\right) * \left(1/\widetilde{R_0}\right)$. The transmitter side compensating capacitor magnitude is given by

$$\begin{cases} C_1 = \dfrac{1}{\omega_P^2 L_{1L} + \omega_P\left(\widetilde{V_0}/I_1\right)\sin(\phi)} \\ \quad = \dfrac{1}{\omega_P^2\left[L_{1L} + \left(L_M/\left\{1 + \omega_P^2\left(L_M/\widetilde{R_0}\right)^2\right\}\right)\right]} \end{cases} \quad (5)$$

The expressions for $\cos(\phi)$ and $\sin(\phi)$ are given in

$$\begin{cases} \cos(\phi) = (\omega_P L_M)/\sqrt{\widetilde{R_0}^2 + (\omega_P L_M)^2} \\ \sin(\phi) = \widetilde{R_0}/\sqrt{\widetilde{R_0}^2 + (\omega_P L_M)^2} \end{cases} \quad (6)$$

In the proposed series compensated WPT system the input voltage V_P is replaced by V_{Cr}. The circuit formed by C_1, L_{1L}, L_M and $\widetilde{R_0}$ is similar to a series *R*–*L*–*C* circuit with its resonant frequency majorly decided by C_1 and L_{1L}. The dc component of V_{Cr} is blocked by C_1 and V_{Cr} frequency is controlled to be close to the resonant frequency of WPT circuit. Owing to the filtering property of C_1–L_{1L} tank the current through transmitter coil will be nearly sinusoidal and most of the analysis done assuming sinusoidal V_P remains valid provided it is replaced by fundamental component of V_{Cr}. The compensated transmitter circuit simply appears as a current source (sink) across C_r. Fig. 7*a* schematically shows a simplified equivalent circuit where the converter is represented by a voltage source (E), inductor (L_r) and capacitor (C_r). The WPT load is represented by a current source (I_1). This will be the exact circuit topology when S_r is off and clamping circuit is ignored. The circuit of Fig. 7*a* helps in qualitative analysis of interaction between the resonant converter and the compensated WPT load. As shown in Fig. 7*b*, the current through L_r and C_r will be due to a voltage source connected in series and due to a current source connected in parallel. The current source may produce a significantly amplified current in the tank circuit formed by L_r and C_r. This effect, as indicated in Section 3, may significantly alter the operating condition of resonant dc link converter.

2.5 Difficulty with series compensation topology

The proposed resonant dc link converter (Fig. 2) for the WPT system, when overloaded, may not be able to produce sustained oscillating voltage across C_r. Each cycle of V_{Cr} oscillation starts with the opening of switch S_r and stops when V_{Cr} resonates back to zero. When V_{Cr} falls to zero, S_r turns on again to recharge the resonant inductor. With turn-off of S_r new cycle of resonating V_{Cr} starts. However, due to overloading V_{Cr} voltage may get sufficiently damped and may not fall to zero. In such a case, switch S_r will not turn-on and oscillating voltage may eventually die out. Fig. 8 shows one such typical simulated waveform where oscillation dies out after a few cycles. Here the circuit parameters are as given in Table 2.

The capacity to handle required WPT (load) current while maintaining oscillation depends on the circuit parameters given in Table 2. These parameters, including I_0 and clamping voltage (KE), also decide the frequency of oscillation. The series compensated circuit, when operating near resonance condition may draw large current from C_r and may overwhelm the dc–dc resonant converter's operation. This results in V_{Cr} oscillations dying out or its frequency gets significantly altered. In either case, the intended operating condition of the WPT system will not be maintained.

In order to reduce interference between the resonant converter and the compensated WPT coil the compensation strategy is changed to series-parallel compensation as shown in Fig. 9. The additional parallel compensating capacitor (C_{11}) provides a shunt

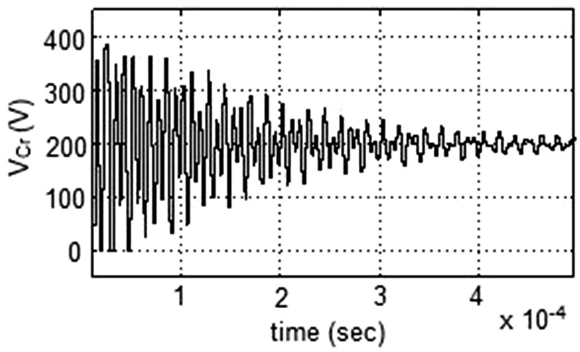

Fig. 8 *Typical waveform of resonant voltage V_{Cr} under overloading*

Table 2 Circuit parameters for simulating resonant converter's output voltage

Parameter	Value	Unit
L_r	28	μH
C_r	60	nF
E	200	V
I_0	5	A
$\widetilde{R_0}$	58.6	Ω
C_1	19.45	nF
L_{1L}	178.61	μH
L_M	30.69	μH
K	1.8	

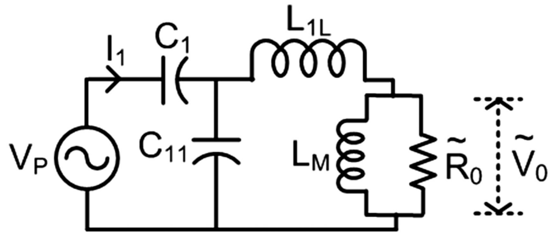

Fig. 9 *Series – Parallel compensation topology*

path for majority of WPT coil's current and the resulting current seen by converter's C_r is significantly reduced. This results in a more stable operation of the converter. The experimental work done by the authors corroborate this. Many results could be obtained using series-parallel compensation and few important ones are presented in Section 4.

3 Effect of misalignment and need for tuning T_X circuit's frequency

In dynamic wireless EV charging system, misalignment between transmitter and receiver coils is expected and the system should be tolerant to such phenomena. Owing to misalignment, the coil's equivalent circuit parameters, including mutual and leakage inductances change. This also changes the resonant frequency of the compensated WPT coil as the compensating capacitors remain the same. In loosely coupled coils the leakage inductance is much more dominant compared to mutual inductance even when the coils are fully aligned. Since the total of mutual and leakage inductances add up to a fixed value (= self-inductance), the percentage change in resonant frequency due to various conditions of misalignment is not much. However, even little mismatch between the converter's output frequency and the resonant frequency of WPT coils create large variation in output power. One simple solution to mitigate the effect of misalignment is to dynamically tune the frequency of the converter's output voltage. Fortunately, the proposed converter (Fig. 2) allows a change in output frequency by varying either the factor 'K' (of clamping voltage) or by changing the switch current

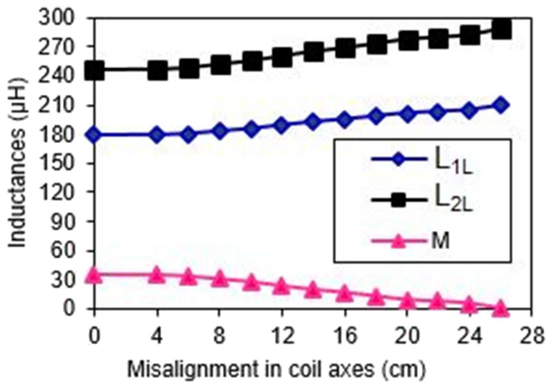

Fig. 10 *Effect of misalignment on various inductances*

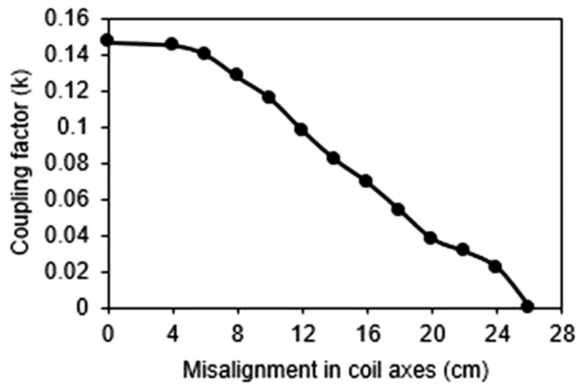

Fig. 11 *Effect of misalignment on coupling factor*

I_0. Both these factors have a bearing on switch ratings which need to be kept in mind.

3.1 Effect of misalignment

In this paper, the transmitter and the receiver coils are assumed to be planer and separated by a vertical distance of 15 cm. The separation in coil-axes is a measure of coil's misalignment. Fig. 10 shows the effect of misalignment on measured values of leakage and mutual inductances. The method of measurement is discussed in Section 2.3. These parameters were also determined by finite element software tools and are generally in agreement.

Fig. 11 shows variation in coupling factor 'k' under misalignment. There is no simple analytical relation between various parameters of coil and misalignment distance.

3.2 Method for tuning converter circuit's output frequency

The resonant frequency of WPT system is sensitive to misalignment and change in load. However, percentage change in this frequency is small and converter's output frequency may be tuned to match with WPT frequency. The authors have proposed two different frequency tuning methods which are:- (i) control over normalised S_r current 'α' ($= I_0\sqrt{(L_r/C_r)}/E$) and (ii) control over K (clamping voltage level). Under no-load condition, fundamental frequency of V_{Cr} (= ω_P rad/s) normalised against $\omega(= 1/\sqrt{L_r C_r})$ is given by (7) and its variation against α and K is plotted in Fig. 12. The expression given in (7) assumes no load across C_r. The derivation of (7) is achieved by suitably modifying similar analysis done in [18] where the load was considered to be a constant dc current sink. No-load condition will also come into this same category. Further, it is found that effect of loading (under design limits) is significantly less in series-parallel compensation topology (when compared with only series compensation).

(see (7))

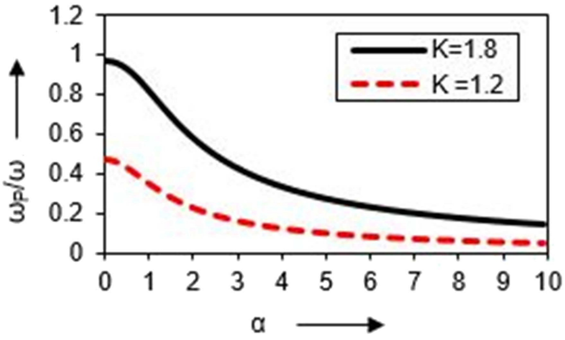

Fig. 12 *Variation in converter's normalised frequency against 'α' and 'K' (under no load)*

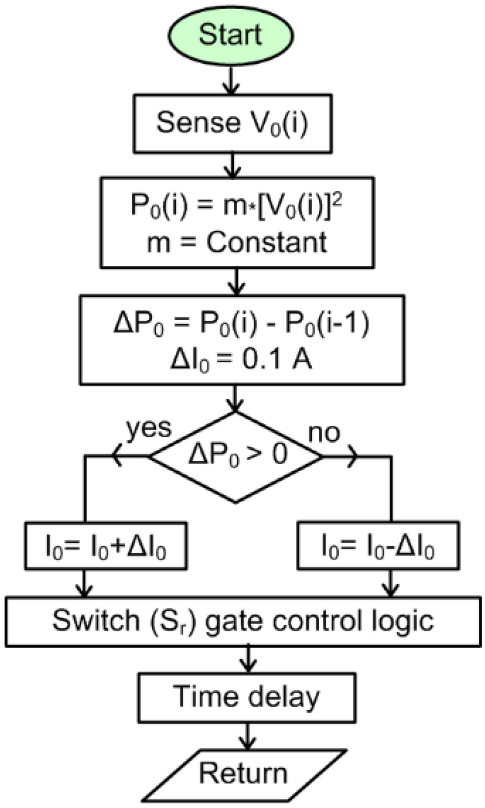

Fig. 13 *Flow chart of MPPT algorithm*

3.3 MPPT arrangement

The active frequency tuning for the proposed resonant converter is done by controlling switch current 'I_0' (within safe limits of switch rating). The control is based on the P & O method of MPPT algorithm. The proposed control algorithm is quite simple and involves only one voltage measurement. The schematic arrangement is shown in Fig. 5. Here it is assumed that the requirement is to always output maximum power from the WPT system. In case EV is already charged to its full capacity, a higher level controller would disconnect the input power. In Fig. 5, the load is denoted by a resistor (R_L) connected across the rectified and filtered receiver side voltage (V_0). Output power (P_0) is proportional to square of V_0 and the algorithm requires only voltage (V_0) measurement. The frequency of the converter is perturbed by perturbing the I_0 reference value (stored in memory) for switch S_r. The flow chart for this MPPT arrangement is shown in Fig. 13. A similar frequency tuning method where perturbation is given in 'K' was also tested. The proposed MPPT schemes are verified experimentally.

4 Experimental verifications

Some experimental results have been presented to validate the working of the proposed WPT system as shown in Fig. 5. Results have been taken both for aligned and slightly unaligned positions of WPT coils. First, the results for the aligned conditions are presented followed by some results under misaligned conditions.

4.1 Coils under aligned position

The transmitter and receiver coils are placed horizontally and their axes are fully aligned. The vertical separation between the coils is 15 cm. The laboratory scale setup is able to transmit about 240 W of output power with an overall system efficiency of around 68%. This efficiency is expected to increase significantly when power levels are increased. The experimental waveforms presented in Figs. 14*a–i* should help explain the working of the proposed WPT system. The circuit operates at around 80 kHz which is the intended operating frequency. The parameters for the experimental results are mentioned in Table 1. The symbols used in Table 1 are the same as in Fig. 5. Load (R_L) on the receiver side is a resistor of

$$\frac{\omega_P}{\omega} = \pi \frac{1}{\left(\sqrt{\alpha^2 - K^2 + 2K/(K-1)}\right) + \tan^{-1}(-\alpha) - \cos^{-1}\left[\left((K-1)/\sqrt{1+\alpha^2}\right)\right] + \alpha} \tag{7}$$

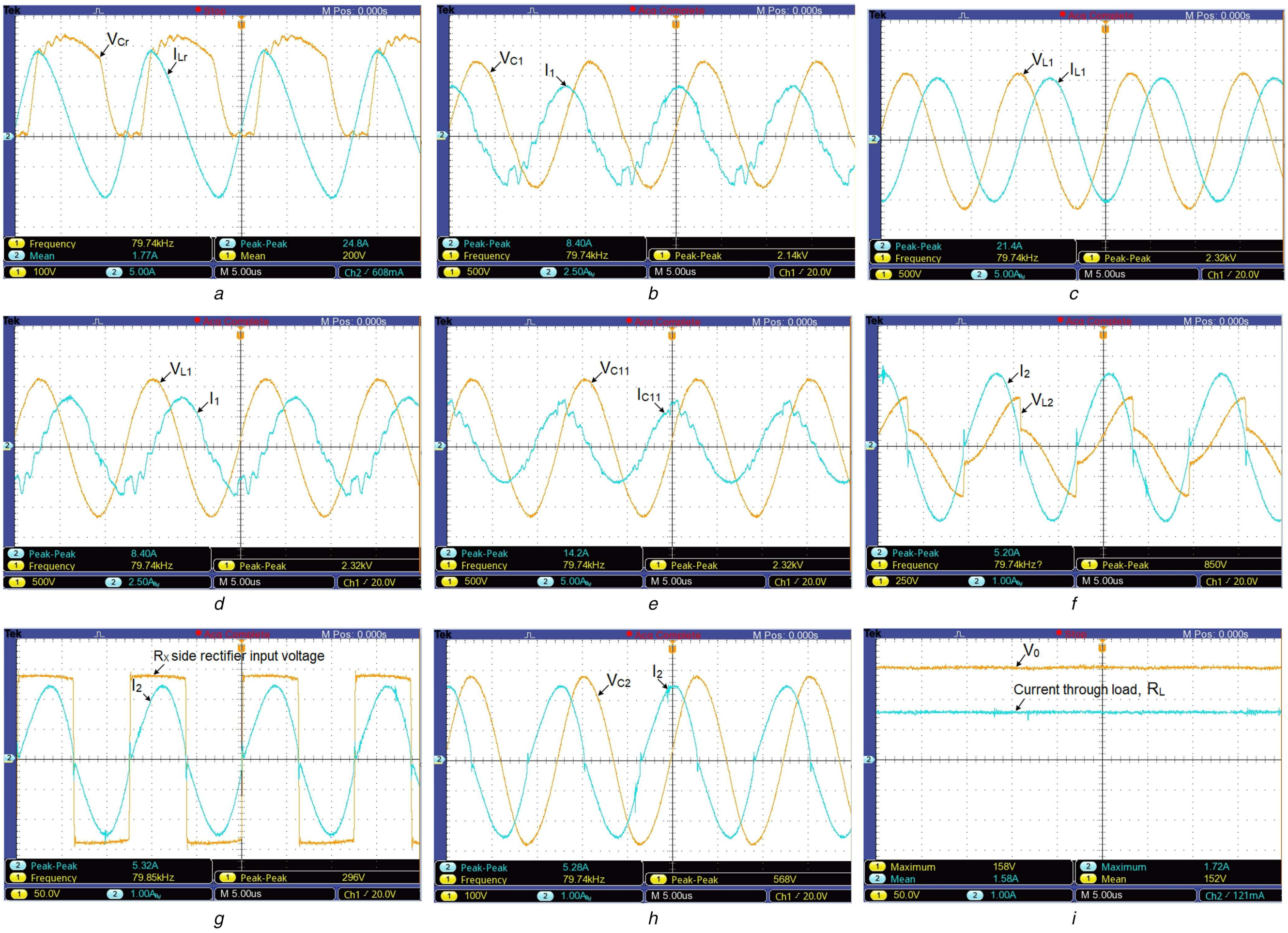

Fig. 14 *Experimental results for WPT system under aligned condition*
(a) Waveforms of resonant circuit's voltage ($V_{\rm Cr}$) and current ($I_{\rm Lr}$): X-axis:1 unit = 5.0 µs, Y-axis ($V_{\rm Cr}$): 1 unit = 100 V and Y-axis ($I_{\rm Lr}$):1 unit = 5 A, ***(b)*** Waveforms of voltage across series compensating capacitor ($V_{\rm C1}$) and current through it (I_1): X-axis: 1 unit = 5.0 µs, Y-axis ($V_{\rm C1}$):1 unit = 500 V and Y-axis (I_1):1 unit = 2.5 A, ***(c)*** Waveforms of transmitter coil's voltage ($V_{\rm L1}$) and current ($I_{\rm L1}$): X-axis:1 unit = 5.0 µs, Y-axis ($V_{\rm L1}$): 1 unit = 500 V and Y-axis ($I_{\rm L1}$):1 unit = 5 A, ***(d)*** Waveforms of transmitter coil's voltage ($V_{\rm L1}$) and current (I_1): X-axis:1 unit = 5.0 µs, Y-axis ($V_{\rm L1}$):1 unit = 500 V and Y-axis (I_1):1 unit = 2.5 A, ***(e)*** Waveforms of voltage across parallel-compensating capacitor ($V_{\rm C11}$) and current through it ($I_{\rm C11}$): X-axis:1 unit = 5.0 µs, Y-axis ($V_{\rm C11}$):1 unit = 500 V and Y-axis ($I_{\rm C11}$):1 unit = 5 A, ***(f)*** Waveforms of receiver coil's voltage ($V_{\rm L2}$) and current (I_2): X-axis:1 unit = 5.0 µs, Y-axis ($V_{\rm L2}$):1 unit = 250 V and Y-axis (I_2):1 unit = 1 A, ***(g)*** Waveforms of rectifier input voltage and current (I_2): X-axis:1 unit = 5.0 µs, Y-axis (Rectifier input voltage):1 unit = 50 V and Y-axis (I_2):1 unit = 1 A, ***(h)*** Waveforms of $\rm R_X$ side series capacitor voltage ($V_{\rm C2}$) and current through it (I_2): X-axis:1 unit = 5.0 µs, Y-axis ($V_{\rm C2}$):1 unit = 100 V and Y-axis (I_2):1 unit = 1.0 A, ***(i)*** Waveforms of load voltage (V_0) and load current: X-axis:1 unit = 5.0 µs, Y-axis (V_0):1 unit = 50 V and Y-axis (Current through load $R_{\rm L}$):1 unit = 1 A

100 Ω. For the digital storage oscilloscope waveforms the current and voltage scales are mentioned below their title lines.

Fig. 14*a* shows $I_{\rm Lr}$ and $V_{\rm Cr}$ waveforms (the clamping capacitor magnitude is only moderately large and hence clamping voltage level is not as flat as in Fig. 3). The dc component of $I_{\rm Lr}$ indicates the input power to the WPT system which is estimated to be around 354 W (while output power to $R_{\rm L}$ is about 240 W). Fig. 14*b* shows voltage across series compensating capacitor ($V_{\rm C1}$) and current through it (I_1). The dc component in $V_{\rm C1}$ equals the input dc voltage (E). Fig. 14*c* shows the transmitter coil's voltage ($V_{\rm L1}$) and current ($I_{\rm L1}$). These waveforms are around 79.7 kHz which is close to WPT system's resonance frequency. Fig. 14*d* shows $V_{\rm L1}$ and I_1 waveforms. The difference between I_1 and $I_{\rm L1}$ flows through the parallel compensating capacitor (C_{11}). Fig. 14*e* separately shows the current and voltage of C_{11}. In Fig. 14*f* receiver coil voltage ($V_{\rm L2}$) and current (I_2) are shown. The abrupt voltage change in $V_{\rm L2}$ is due to reflected voltage across rectifier input. The rectifier input voltage and current waveforms are shown together in Fig. 14*g*. As the current direction changes the rectifier-diode conduction pattern also changes and the reflected voltage at the input of rectifier reverses. Fig. 14*h* shows the $\rm R_X$ side series capacitor voltage ($V_{\rm C2}$) and current through it. Fig. 14*i* shows the load voltage (V_0) and load current. From these outputs, power P_0 is estimated to be around 240 W.

4.2 Coils under misaligned position

Owing to misalignment, the coupling factor between the $\rm T_X$ and $\rm R_X$ coils change as illustrated in Fig. 11. The resonant frequency of the WPT coils also decreases slightly as leakage inductance increases and mutual inductance reduces. The converter which was tuned for the aligned condition may not work optimally under misalignment. Slight retuning of the converter's frequency may be required. Fig. 15*a* shows the variation in output voltage (V_0) and envelope of $\rm R_X$ coil current (I_2) for different misalignments. Here misalignment between the coils' axes is created by moving the receiver coil in the horizontal plane manually. The distance between the coil axes is taken as a measure of misalignment. In Fig. 15*a* misalignment is maximum (15 cm) for extreme left point and is 0 cm for extreme right point. Due to manual control, the misalignment distance may not have changed uniformly with time. However, the marking below the current envelope gives an approximate idea of misalignment distance. For Fig. 15*a* MPPT algorithm is not implemented but still, some variation in converter's frequency is observed, mainly due to change in impedance of the WPT coil. Fig. 15*b* shows a plot of

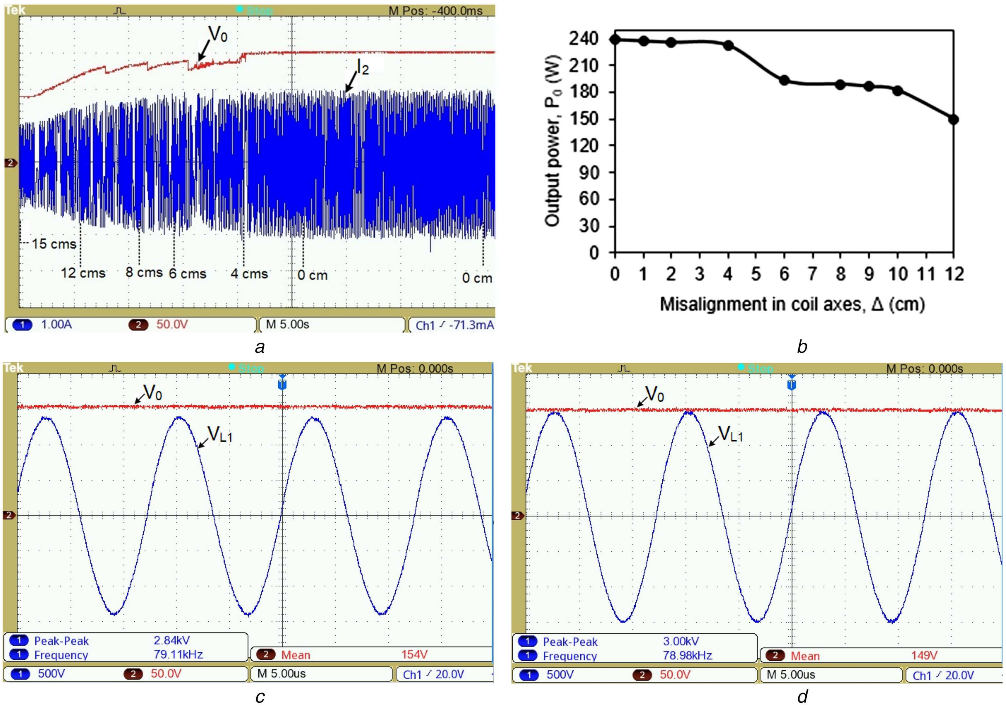

Fig. 15 *Experimental results for WPT system under misaligned condition*
(a) Effect of misalignment on output voltage (V_0) and receiver coil current (I_2): X-axis:1 unit = 5.0 s, Y-axis (V_0):1 unit = 50 V and Y-axis (I_2):1 unit = 1 A, ***(b)*** Plot of output power (P_0) versus misalignment distance without active frequency tuning of converter, ***(c)*** Transmitter coil's voltage (V_{L1}) and output voltage (V_0) under active frequency tuning at misalignment distance, Δ = 6 cm: X-axis:1 unit = 5.0 µs, Y-axis (V_{L1}):1 unit = 500 V and Y-axis (V_0):1 unit = 50 V, ***(d)*** Transmitter coil's voltage (V_{L1}) and output voltage (V_0) under active frequency tuning at misalignment distance, Δ = 8 cm: X-axis:1 unit = 5.0 µs, Y-axis (V_{L1}):1 unit = 500 V and Y-axis (V_0):1 unit = 50 V

experimentally obtained output power for different misalignment distances.

As can be seen in Fig. 15*b* the output power reduces as misalignment increases. At 6 and 8 cm of misalignment the output power values are 193 and 189 W, respectively. Next converter's frequency is re-tuned with the help of MPPT controller and the new power values are 237 and 222 W, respectively. The corresponding frequencies are ∼79.1 and 79 kHz, respectively. The $\cos(\phi)$ magnitude as given by (6) decreases with increased misalignment and the effective impedance of WPT coil under perfect compensation [proportional to $\cos(\phi)^2 * \widetilde{R_0}$] decreases. For the same input voltage the current and voltage of transmitter coil increases. In spite of increased current of transmitter coil, the R_X side current and output power may not increase due to decreased coupling factor between coils. This effect is captured in Figs. 15*c* and *d* which show the transmitter coil's voltage (V_{L1}) and output voltage (V_0). The load connected across V_0 is a fixed resistor of around 100 Ω. As observed from Figs. 14*c* and *d* the aligned condition T_X coil's voltage (peak-to-peak) is 2.32 kV while it is 2.84 kV for 6 cm of misalignment (Fig. 15*c*) and 3 kV for 8 cm of misalignment (Fig. 15*d*).

5 Conclusions

The authors have suggested a new method for powering a WPT system. A resonant converter with low switching losses has been suggested and analysed. The converter structure is simple and employs less number of switches. These switches operate under zero voltage switching condition. The proposed converter is also suitable for dynamic tuning of the output frequency. The method of converter operation and output frequency tuning has been explained. Effect of misalignment has been brought out and it is shown that misalignment or change in load results in change of WPT coil's parameters. The changed parameters call for returning of converter's output frequency such that the resonant frequency of compensated WPT coils remain closely matched. The suggested remedial method for overcoming the effect of misalignment is quite simple and easy to implement. Sufficient experimental results are presented to validate the proposed circuit operation.

6 References

[1] Wang, C.S., Covic, G.A., Stielau, O.H.: 'Investigating an LCL load resonant inverter for inductive power transfer applications', *IEEE Trans. Power Electron.*, 2004, **19**, (4), pp. 995–1002

[2] Sallan, J., Villa, J.L., Llombart, A., *et al.*: 'Optimal design of ICPT systems applied to electric vehicle battery charge', *IEEE Trans. Ind. Electron.*, 2009, **56**, (6), pp. 2140–2149

[3] Miller, J.M., Onar, O.C., Chinthavali, M.: 'Primary-side power flow control of wireless power transfer for electric vehicle charging', *IEEE J. Emerg. Sel. Top. Power Electron.*, 2015, **3**, (1), pp. 147–162

[4] Shin, J., Shin, S., Kim, Y., *et al.*: 'Design and implementation of shaped magnetic-resonance-based wireless power transfer system for roadway-powered moving electric vehicles', *IEEE Trans. Ind. Electron.*, 2014, **61**, (3), pp. 1179–1192

[5] Buja, G., Bertoluzzo, M., Dashora, H.K.: 'Lumped track layout design for dynamic wireless charging of electric vehicles', *IEEE Trans. Ind. Electron.*, 2016, **63**, (10), pp. 6631–6640

[6] Wang, Z., Cui, S., Han, S., *et al.*: 'A novel magnetic coupling mechanism for dynamic wireless charging system for electric vehicles', *IEEE Trans. Veh. Technol.*, 2018, **67**, (1), pp. 124–133

[7] Fujita, T., Yasuda, T., Akagi, H.: 'A dynamic wireless power transfer system applicable to a stationary system', *IEEE Trans. Ind. Appl.*, 2017, **53**, (4), pp. 3748–3757

[8] Zhu, Q., Wang, L., Guo, Y., *et al.*: 'Applying LCC compensation network to dynamic wireless EV charging system', *IEEE Trans. Ind. Electron.*, 2016, **63**, (10), pp. 6557–6567

[9] Gil, A., Sauras-Perez, P., Taiber, J.: 'Communication requirements for dynamic wireless power transfer for battery electric vehicles'. Proc. Int. Conf. Electric Vehicle, Florence, December 2014, pp. 1–7

[10] Echols, A., Mukherjee, S., Mickelsen, M., *et al.*: 'Communication infrastructure for dynamic wireless charging of electric vehicles'. Proc. Conf. Wireless Communications and Networking, San Francisco, CA, May 2017, pp. 1–6

[11] Naberezhnykh, D., Reed, N., Ognissanto, F., *et al.*: 'Operational requirements for dynamic wireless power transfer systems for electric vehicles'. Proc. Int. Conf. Electric Vehicle, Florence, December 2014, pp. 1–8

[12] Sokal, N.O., Sokal, A.D.: 'Class E-A new class of high-efficiency tuned single-ended switching power amplifiers', *IEEE J. Solid-State Circuits*, 1975, **10**, (3), pp. 168–176

[13] Rivas, J.M., Han, Y., Leitermann, O., *et al.*: 'A high-frequency resonant inverter topology with low voltage stress', *IEEE Trans. Power Electron.*, 2008, **23**, (4), pp. 1759–1771

[14] Divan, D.M.: 'The resonant DC link converter-a new concept in static power conversion', *IEEE Trans. Ind. Appl.*, 1989, **25**, (2), pp. 317–325

[15] Hayati, M., Roshani, S., Roshani, S., *et al.*: 'Design of class E power amplifier with new structure and flat top switch voltage waveform', *IEEE Trans. Power Electron.*, 2018, **33**, (3), pp. 2571–2579

[16] Choi, J., Tsukiyama, D., Tsuruda, Y., *et al.*: 'High-frequency, high-power resonant inverter with eGaN FET for wireless power transfer', *IEEE Trans. Power Electron.*, 2018, **33**, (3), pp. 1890–1896
[17] Aldhaher, S., Luk, P.C.K., Whidborne, J.F.: 'Tuning class E inverters applied in inductive links using saturable reactors', *IEEE Trans. Power Electron.*, 2014, **29**, (6), pp. 2969–2978
[18] Divan, D.M., Skibinski, G.: 'Zero-switching-loss inverters for high-power applications', *IEEE Trans. Ind. Appl.*, 1989, **25**, (4), pp. 634–643
[19] Chen, C., Xu, X., Divan, D.M.: 'Conductive electromagnetic interference (EMI) noise evaluation for an actively clamped resonant DC link inverter (ACRDCLI) for electric vehicle (EV) traction drive applications'. Proc. Int. Conf. Industry Applications, New Orleans, LA, USA, October 1997, pp. 1550–1557
[20] Liu, J., Chan, K.W., Chung, C.Y., *et al*.: 'Single-stage wireless-power-transfer resonant converter with boost bridgeless power-factor-correction rectifier', *IEEE Trans. Ind. Electron.*, 2018, **65**, (3), pp. 2145–2155
[21] Moradewicz, A.J., Kazmierkowski, M.P.: 'Contactless energy transfer system with FPGA-controlled resonant converter', *IEEE Trans. Ind. Electron.*, 2010, **57**, (9), pp. 3181–3190
[22] Zhang, W., Mi, C.C.: 'Compensation topologies of high-power wireless power transfer systems', *IEEE Trans. Veh. Technol.*, 2016, **65**, (6), pp. 4768–4778

7 Appendix

7.1 Interactive driver assistance system

The DWC for EV must incorporate the driver assistance system to maintain the desired orientation of the vehicle. Road markings and pole mounted camera-based object identification techniques etc., may be incorporated. Apart from these some additional sensors embedded on the road surface may help communicate with the driver. Arrays of piezoelectric pressure sensors or electro-mechanical limit switches may be incorporated to ascertain the lateral misalignment of the vehicle. The authors have tested a preliminary communication system using Zigbee module to wirelessly communicate the vehicle position. However, the results are too basic and are not being presented here.